Massimiliano Fraldia,∗, Arsenio Cutoloa, Angelo Rosario Carotenutoa, Stefania Palumboa, Nicola Pugnob,c
a Department of Structures for Engineering and Architecture, University of Napoli Federico II, Italy
b Laboratory of Bio-inspired, Bionic, Nano, Meta Materials and Mechanics, Department of Civil, Environmental and Mechanical Engineering, University of Trento, Italy c School of Engineering and Materials Science, Queen Mary University of London, UK

A B S T R A C T

The progressive falling of barriers among disciplines is opening unforeseen scenarios in diagnosis and treatment of cancer diseases. By sharing models and mature knowledge in physics, engineering, computer sciences and molecular biology, synergistic efforts have in fact contributed in the last years to re-think still unsolved problems, shedding light on key roles of mechanobiology in tumors and envisaging new effective strategies for a precise medicine. The use of ultrasounds for altering cancer cells' program is one of the most attracting grounds to be explored in oncophysics, although how to administer mechanical energy to impair selected cell structures and functions simultaneously overcoming the critical trade-off between the impact of the cure and the patient risk still remains an open issue. Within this framework, by starting from the theoretical possibility of selectively attacking malignant cells by exploiting the stiffness discrepancies between tumor and healthy single cells, first proposed by Fraldi et al. (2015), we here investigate the in-frequency response of an overall spherical close-packing of geometrically equal polyhedral cells to gain insights into how mechanical resonance and vibration-induced failure phenomena can be oriented to destroy specific target units when both the cell populations coexist, as it happens for *in vivo* cases. Inspired by the dynamic action of earthquakes – which fracture only selected elements among adjacent ones in the same structure or damage individual constructions in contiguous buildings – we study the harmonic response of hierarchically architectured cell agglomerates, inhabited by both tumor and healthy cells that interact mutually throughout the extra-cellular matrix and whose cytoskeleton is modeled as a nonlinear soft-tensegrity structure. Numerical Finite Element results show that, at frequencies compatible with low intensity therapeutic ultrasounds, mechanical resonance and possible fatigue cycles of the pre-stressed actin filaments and microtubules can be selectively induced in cancer cells as a function of the global volume fraction of the cell species, paving the way for future engineered treatment protocols.

1. Introduction

Oncological treatments are to date based on several therapeutic strategies that involve surgical techniques, radiotherapy, chemo- and systemic therapies. These invasive interventions often entail side effects that compromise the quality of life of patients. The optimal treatment of solid tumors should ideally induce irreversible death of cancer cells by preserving the surrounding healthy tissue through the adoption of miniinvasive strategies. With this scope, avant garde procedures have been recently proposed to replace or at least limit the use of some current therapeutic protocols and reduce adverse consequences during the course of the disease. Among them, the adoption of ultrasounds (US) for Treatments based on High Intensity Focused Ultrasounds (HIFU) induce the thermal ablation of confined regions occupied by the malignant cells, by severely damaging tumor vascular networks and thus compromising nutrient supply and cell proliferation (Wu, 2004). The long-term clinical results demonstrate an encouraging efficacy with contained side effects, that however include cases of infection, skin burns and tissue damages. Then, great attention has been addressed to the study of Low Intensity Therapeutic Ultrasounds (LITUS) in cancer therapy (Wood and Sehgal, 2015; Tijore et al., 2020). The LITUS, characterized by intensities below the 5 W per square centimeter, are reputed safe and can be easily applied to solid tumors by means of relatively inexpensive apparatuses. Their application, following the *in vitro* and *in vivo* observations from the literature, can be involved in many strategies of cancer therapy: the sonodynamic therapy, to stimulate intratumoral sensitizing molecules, and the ultrasound-mediated chemotherapy, to enhance drug delivery or to destroy agent-loaded microbubbles transported in the tumor (Wood and Sehgal, 2015; Tomizawa et al., 2001). Other emerging protocols provide the use of LITUS to target DNA-loaded microbubbles, carried in tumor vessels, in order to induce gene transfection of nucleic acids in tumor parenchyma, the ultrasounds having a key role also in altering the pore permeability of cells and capillaries to let the infiltration of the genetic material (sonoporation) (Wood and Sehgal, 2015; Haag et al., 2006; Li et al., 2014). LITUS have been used also to stimulate antivascular thermal effects and to induce cavitation of micro-particles driven at the tumor sight (Wood et al., 2005). In all these experimentations, consistent effects in terms of cancer cell death were produced, but almost the whole of the described methods represent US-mediated processes in which insonation is employed to trigger and facilitate other phenomena, thus somehow underestimating the potential to obtain the mechanical disruption of tumor cells as a direct effect of the cytostructure vibration caused by the US waving. This is probably due to the fact that the biophysics underlying the nonthermal interaction mechanisms among living cells systems and US fields is not as well established as the knowledge of the way in which focused irradiation can produce thermal loading, cavitation effects and the excitation of micro-(nano-) particles (Baker et al., 2001). In fact, to the best authors' knowledge, although the effects of low intensity US on the apoptosis and gene expression of cell cultures have been studied (Tian et al., 2005; Tabuchi et al., 2008; Feng et al., 2008; Sawai et al., 2012), strategies to selectively attack tumors by exploiting the sole mechanical energy carried by LITUS, based on the direct characterization of the structural response of cancer cells in multi-cell agglomerates to dynamic actions, have been not yet investigated. This would require a more detailed mechanical characterization of both tumor and healthy micro-environments, from the single-cell level up to the macroscale of the solid tumor bodies. Currently, many efforts are being spent to better understand how biological soft matters react to mechanical stimuli induced by ultrasounds, by in particular focusing on the effects of the US on the structures of human cells, significantly influenced by the frequency and the applied energy density (Schuster et al., 2013). Experimental results showed that, in specific ranges of energy and frequencies, US effects are different if directed on either malignant or healthy cells. An increase in both healthy cells proliferation and cancer cells apoptosis is highlighted in several works, in which the relation between US excitation and cell biological response is however not completely clear (Schuster et al., 2013; Chumakova et al., 2006; Lejbkowicz and Salzberg, 1997; Lejbkowicz et al., 1993). On the other hand, it is therein indicated that malignant cells can be highly sensitive to ultrasonic irradiation with respect to normal ones, this suggesting that low-intensity ultrasounds could be helpfully exploited for cancer treatment (Lejbkowicz and Salzberg, 1997). In this scenario, cyto-mechanics surely plays a primary role for characterizing the response of cells to US, which can activate remodeling processes of cell cytoskeleton, as also experimentally observed in the case of human airway smooth muscle cells (Mizrahi et al., 2012).

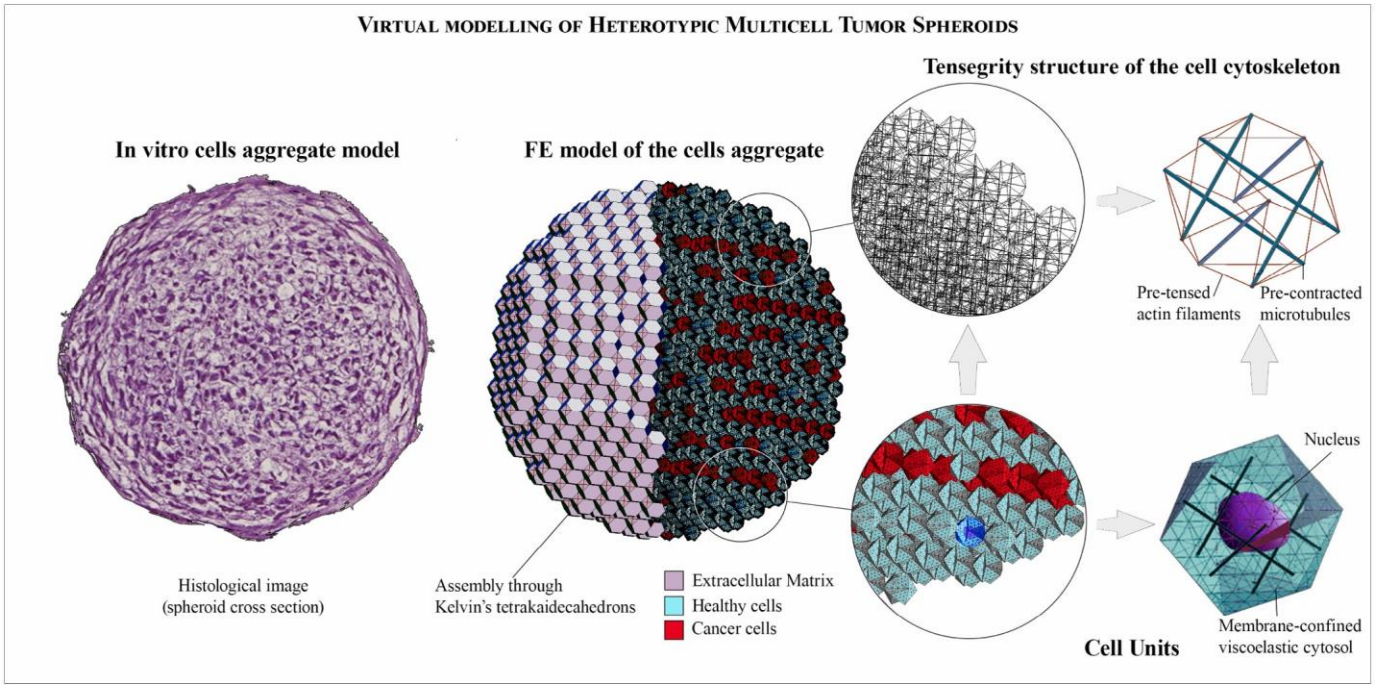
VIRTUAL MODELLING OF HETEROTYPIC MULTICELL TUMOR SPHEROIDS
Tensegrity structure of the cell cytoskeleton
In vitro cells aggregate model
FE model of the cells aggregate
Pre-tensed actin filaments
Pre-contracted microtubules
Nucleus
Histological image (spheroid cross section)
Assembly through Kelvin's tetrakaidecahedrons
Extracellular Matrix
Healthy cells
Cancer cells
Cell Units
Membrane-confined viscoelastic cytosol

Fig. 1. Synoptic panel illustrating the virtual model of the hierarchical organization of the spherical cell aggregate, whose dynamics is analyzed in terms of harmonic response. (*Left*) Histological image of an *in vitro* spheroidal aggregate of cells. (*From center to right*) Virtual three-dimensional FE model of the cells aggregate inhabited by both malignant and normal cells (middle) with extracellular matrix and cell units (in red the cancer cells). The spheroid is composed by geometrically equal building blocks, each of them being formed by an ECM-surrounded cell, which can represent tumor or normal phenotypes, characterized by a membrane confining the cytosol in which a central nucleus is imprisoned by the cell cytoskeletal structure, modeled as a 30-element tensegrity (see details on the right).

With these premises, the idea of selectively attacking cancer cells by using mechanical stimuli has been for the first time highlighted in a recent work by Fraldi et al. (2015), who theoretically demonstrated that healthy and cancer cells exhibit a distinct sensitivity to ultrasound irradiation. In the aforementioned work, by starting from well-established experimental evidences according to which a wide variety of tumor and healthy cells of the same lineage have a different stiffness (Lekka et al., 2012; Prabhune et al., 2012; Faria et al., 2008; Cross et al., 2007; Lekka et al., 1999; Korayem et al., 2018b,a; Korayem and Rastegar, 2019; Korayem et al., 2020), the malignant cells resulting on average 1.7 times more compliant than the normal ones, the authors used generalized visco-elastic elements to model both cancer and healthy cells, which could be discriminated in terms of their in-frequency response (from tens to hundreds of kHz). In fact, the tumor and healthy counterparts, independently of the cell line, showed distinct resonance-like maxima in response to LITUS-induced oscillations. This key result was actually a fundamental step to envisage mechanically-based strategies to selectively target and attack tumor cells by avoiding risks for the healthy ones (Fraldi et al., 2015). The model has been successively updated by including the influence of the intrinsic nonlinearity of the cytoskeleton filaments and the effects of their pre-stretch in the computation of the actual stiffness of adherent cells, in a way to analyze the effects of both cytoskeleton remodeling and intracellular pre-stress on the harmonic response of cells by means of a generalized fractional-derivative based model and a small-on-large approach (Fraldi et al., 2017). These works outlined the potential to determine fatigue-like phenomena able to produce damaging in tumor cells through a purely mechanical action. In line with these findings, Geltmeier et al. (2015) developed a numerical model to characterize the dynamic behavior of breast cancer cells under oscillating pressures, the obtained outcomes being supported by *in vitro* experiments, in which 2D and 3D cell cultures were treated with low-frequency ultrasounds also in combination with chemotherapeutic agents, by evidencing different cytotoxic effects between tumor and normal cell types. Successive literature works reverberated the possibility of using low-intensity ultrasounds as an alternative strategy to attack cancer cells. In fact, with analogous scopes, Heyden and Ortiz (2016) dubbed as oncotripsy the process of applying US to ablate cancer cells at their resonance frequencies, and, by estimating cells eigenfrequencies, they developed a numerical model to describe the dynamics of the single-cell under resonant harmonic excitation (Heyden and Ortiz, 2017, 2016). The effectiveness of this approach was then explored through *in vitro* tests investigating impairments in suspended neoplastic cells produced by the application of low-intensity pulsed ultrasounds (LIPUS) at frequencies below 1MHz and pulse durations above 20 ms (Mittelstein et al., 2020), such outcomes being corroborated by a dynamical model developed to describe damage accumulation within cells under vibration (Schibber et al., 2020). All these works suggest a concrete feasibility in prospecting a mechanically-based strategy to treat localized solid tumors by means of LITUS and indicate that greater efforts should be made to provide a deeper understanding of the tumor and healthy cells mechanical behavior, in order to unveil the US–cell structure interaction. In this sense, to conceive biomechanics-aided innovative treatments of solid tumors, the first evident limit exhibited by the above discussed models is that they all refer to the single-cell scale, often in suspension. As a consequence, to translate *in vivo* these results, one fundamental step is to extend the analyses to cells aggregates. Therefore, the aim of the present work is to study the sonodynamics of a hierarchically-built model of heterotypic multicellular spheroids, in which healthy and tumor cells coexist with different percentages. The response to mechanical vibrations of such systems is analyzed in order to envisage the possibility of predicting the optimal frequencies at which the efficacy of US treatments on entire solid tumors at a certain stage can be maximized in terms of selective damaging of cancer cells that share the environment with healthy cells. To this purpose, threedimensional tumor aggregates are virtually built through an *ad hoc* parametric finite element (FE) procedure, in which each single cell is modeled by including its most mechanically-relevant components. In the literature (Heyden and Ortiz, 2016; Geltmeier et al., 2015), the sole cell elements considered to this aim are the nucleus, the cytoplasm and the membrane, somehow neglecting the active role played by the mechanical response of cell cytoskeleton except in the form of amorphous random network of unstressed fibers (Schibber et al., 2020). Importantly, cell cytoskeleton (CSK) is here included by adopting a 30element tensegrity structure (TS), according to the approach proposed by Ingber (1993). Recently, TS systems have been enriched by considering *soft* paradigms that provided large deformations and constitutive nonlinearities of the elements (Palumbo et al., 2018), by characterizing the nonlinear behavior of single-cell cytoskeleton undergoing large motions during cells reconfigurations (Fraldi et al., 2019). The enhanced TS model actually helped to highlight the primary influence of CSK pre-stress in determining the mechanical response of different cells. In fact, the modeling of nonlinear microfilaments and microtubules allowed to reproduce the distinct stiffness exhibited by normal and malignant cells on the basis of the pre-stretch levels stored in the TS structure (Fraldi et al., 2019). By starting from these recent results, here the finite element model of a system comprising both tumor and healthy cells is generated by considering a properly pre-stressed TS, enveloped by a membrane and confined by a viscoelastic gel-like media (the cytosol), with a central nucleus having higher density. Also, the cell system is coupled to a layer of extra-cellular matrix (ECM), in this way obtaining the periodic unit of the aggregate. Three-dimensional heterotypic tumor spheroids are then generated by means of a custommade procedure that disposes the different units in space according to random-based rules and respecting prescribed tumor dimensions and percentages. Optimal tessellation of the 3D region occupied by the full spheroid is realized by adopting the Kelvin's tetrakaidecahedron (KTKs) to model the shape of the cell-ECM periodic unit. These *in silico* hierarchical models, built up according to the synoptic scheme illustrated in Fig. 1 and in detail described in what follows, were thus used to verify if selective discrimination between tumor and healthy cells can be established at the cells' aggregate level as well, in this way overcoming the limitations related to the analyses of singlecell systems. In combination with the biomechanical analysis of solid tumor growth (Guiot et al., 2006; Carotenuto et al., 2018; Fraldi and Carotenuto, 2018; Carotenuto et al., 2021) and residual stress-induced remodeling (Carotenuto et al., 2019), it is felt that the theoretical predictions of critical frequencies that put into vibration selectively cancer cells in aggregates at different stages of tumor progression could highly impact on possible therapeutic applications of LITUS in cancer treatments.

2. Methods

Three-dimensional agglomerates inhabited by tumor and healthy cells in different percentages and the extra-cellular matrix have been generated by providing a bottom-up approach in which the intra- and extra-cellular structures are assembled in order to form the mechanical sub-units of the aggregate. To this aim, a comprehensive architecture of the cell is conceived, constituted of all its most significant structural elements and immersed in the pericellular environment. The entire model – following the scheme proposed in Fig. 1 – has been step-bystep developed at two scale levels: the single-cell (microscopic) level, considering the interaction between the cell and the ECM, and the cell aggregates level, at which all the cells interact within the environment. The elastic behavior of each constituent has been also properly modeled, and specific topological choices have been made to optimize the dense packaging of the sub-units during the 3D reconstruction procedure. The FE aggregate model has been developed with the aid of Ansys® code (Ansys 15.0 User's Manual, 2013), by writing custom made algorithms in APDL language to define the geometry and the constitutive properties of the components, and to establish the cancer stage, by imaging different fractions of cancer cells within each tumor mass. The scale-specific description of the characteristics of the several sub-structures is reported below.

2.1. Modeling of single-cells and sub-structures

At the single-cell scale, the most mechanically relevant cell components – that concur in determining its overall mechanical response – are: the internal nucleus, the cytosol, the cytoskeleton and the cell membrane, which are primary sites of the most of cellular processes whose alteration is prodromal to tumorigenesis (Ong et al., 2020; Chen, 2017; Innamorati et al., 2011; Carotenuto et al., 2020; Pezo and Singer, 2008). The CSK architecture is here modeled according to the well known 30-element tensegrity (TS) paradigm (Ingber et al., 2014; Ingber, 1993), also very recently reformulated in a finite strain

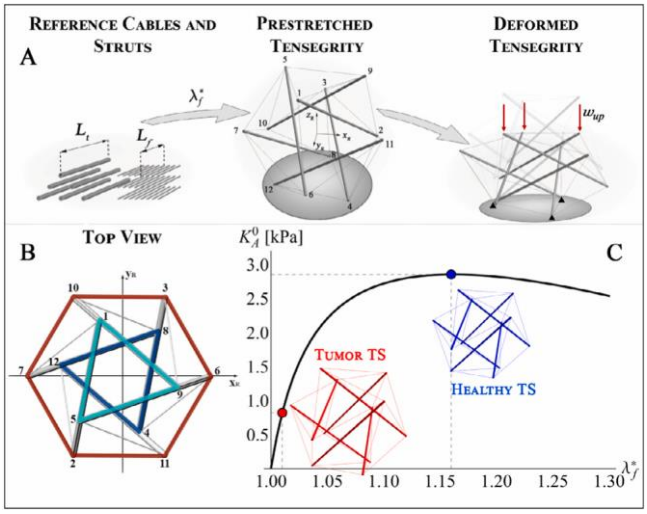

Fig. 2. Construction of the tensegrity model and determination of its axial response.
A. (*Left*) The disassembled elements of the tensegrity in the reference configuration.

{ }

(*Middle*) The 30-element tensegrity in the Cartesian coordinate system x_R, y_R, z_R, governed by the pre-stretch λ^*_f. (*Right*) Loading of the structure to determine the elastic response. B. 30-element tensegrity in a top view showing the chiral symmetry of the structure. C. Analysis of the tangent axial stiffness with varying pre-stretch: in particular the red and blue markers indicate the values of pre-stretch chosen to reproduce the different cytomechanical properties of tumor and healthy cells, respectively.

regime (Fraldi et al., 2019). The TS structure is then immersed in a plasmatic membrane-confined cytosol with (visco-)elastic properties, additionally including the nucleus as a central region with higher density, as shown in Fig. 1.

2.1.1. The tensegrity-based model for cytoskeleton

Preliminary determination of the tensegrity response. The mechanical response of the cell is mainly determined by its cytoskeleton, which provides structural stability and plays a pivotal role into influencing some of its physiological events like migration and mitosis, during which cells dynamically re-arrange their morphology. Tensegrities have been largely used in literature as qualitative paradigm of the cell cytoskeletal structure, because they constitute self-equilibrated architectures which can store elastic energy, called in play during the aforementioned biochemical processes (Ingber et al., 2014). In our model, tensegrity is effectively employed as a predictive instrument to reproduce the mechanical response of the CSK of both healthy and tumor cells, whose distinct stiffness can be modeled by regulating the level of TS prestretch (Fraldi et al., 2019). In particular, the 30-elements tensegrity modules here considered present a regular icosahedral geometry in a pre-stretched configuration, guaranteeing the TS stable equilibrium, see Fig. 1. The topology of each TS unit is defined by the sets of the vertices and the edges, say V_{TS} and E_{TS}:

$V_{TS} = \{1,2,\dots,12\}$,

(1) $E_{TS} = C_{TS} \cup S_{TS}$, $C_{TS} = \{1,2,\dots,24\}$, $S_{TS} = \{25,\dots,30\}$ where C_{TS} and S_{TS} denote the continuous set of cables and the disjointed set of struts, respectively. Indeed, each TS configuration is determined by the twelve nodal Cartesian coordinates of the disjointed struts, say $\mathbf{p}_k (k \in V_{TS})$, to which the actin microfilaments (mFs) are

connected, the origin of the system being placed at the center of the sphere circumscribing all the nodes in a way that the position vector of the vertices are obtainable from rigid motions (see the Appendix). As visible in Fig. 2A, six identical pre-contracted struts with length L^*_t model the cytoskeletal micro-tubules (mTs), while 24 identically preelongated cables, with length L^*_f, are assembled in a way to mimic the mechanical behavior of the mFs.

This symmetric geometry returns a cell TS structure circumscribedv by a sphere of $5L^*_t/4$ in radius, subjected to the additional compatibility constraint:

v

$L^*_f = \sqrt{46}\, L^*_t$ (2)

the subscript f and t denoting the filaments and the tubules, respectively. Furthermore, in the pre-stretched and unloaded configuration, one has that $L^*_f = \lambda^*_f L_f$ and $L^*_t = \lambda^*_t L_t$, where L_f and L_t are the rest lengths of the filaments and tubules in the disarranged reference configuration, respectively, while $\lambda^*_f > 1$ and $\lambda^*_t < 1$ are the relative prestretches (Fig. 2A). In the pre-stretched and unloaded configuration, equilibrium along the z direction gives a relation between the cables and struts axial forces N^*_f and N^*_t:

v

$N_t^* = -6N_f^*$, (3)

while equilibria along the x and y axes are automatically satisfied due to the geometrical symmetry (see the Appendix). By setting the geometrical and constitutive properties of mTs and mFs, according to the literature experimental values reported in Table 1, different configurations can be obtained by modulating the cable pre-stretch λ_f^* (Fraldi et al., 2019). In fact, the effective tangent stiffness exhibited by the nonlinear tensegrity under an external loading will also depend on such pre-stretch value. More in detail, the nonlinear deformation of the TS-modeled cells is taken into account by adopting true strain $\varepsilon_j = \ln\lambda_j$, while each TS bar is assumed to obey a Hencky-type linear constitutive law, so that its Kirchhoff stress is proportional to the strain through the sole Young modulus E_j, i.e. $\tau_j = E_j\varepsilon_j$ under the hypothesis of unloaded lateral surfaces. The energy of the structure reads:

$$\Psi = \frac{1}{2}\sum_{j\in ETS} V_j\tau_j\varepsilon_j = \frac{A_f E_f L_f}{2}\sum_{j\in CTS}\ln^2\left(\frac{l_j}{L_f}\frac{1}{\lambda_f^*}\right) + \frac{A_t E_t L_t}{2}\sum_{j\in TS}\ln^2\left(\frac{l_j}{L_t}\frac{1}{\lambda_t^*}\right) \quad (4)$$

where A_j represents the reference cross-sectional area of the elements and l_j represents the current length exhibited by the jth element as the effect of its elastic deformation due to an imposed action, which moves the whole structure towards an updated configuration identified by the strut vertices $\mathbf{p}'_k = \mathbf{p}_k + \mathbf{v}_k$, the vectors $\mathbf{v}_k = \{u_k, v_k, w_k\}$ denoting the (Cartesian) nodal displacements so that the jth element of the tensegrity has length $l_j = \gamma_j(\mathbf{v}_k)$, see also Fig. 2A. The values of these unknown displacements – defined in a way to preserve symmetry during the deformation (see the Appendix) – can be found by

solving the unconstrained minimization problem $\mathbf{v}_i = \min_{\mathbf{v}_i}\Psi$. More in particular, to mimic the experimental tests performed for measuring the single cells stiffness by means of Atomic Force Microscopy (AFM) techniques (Lekka et al., 2012; Prabhune et al., 2012; Faria et al., 2008; Cross et al., 2007; Lekka et al., 1999), the TS contraction has been examined by prescribing a vertical displacement w_{up} to the nodes 1, 5 and 9 of the tensegrity, that delimit the upper triangular basis (see Fig. 2A and B), while the nodes of the lower basis are all fixed. The numerical solution of the nonlinear system given by the minimization problem has been obtained by the aid of the computational software *Mathematica*® (Wolfram Research, Inc., 2015). The stress–strain response of the tensegrity has been studied in terms of its effective axial stiffness K_A^0, defined as:

$$K_{A0}(\lambda_f^*) = \left[\sum_{up} A_{up}\,\partial w^2\Psi_{up}\right]_{|\mathbf{v}_i|}\Big|_{w_{up}\to 0} \quad (5)$$

that naturally depends on the value of the pre-stretch λ_f^*, as also shown in Fig. 2C with reference to the data reported in Table 1. Importantly, the mechanical response of the tensegrity structure well reproduces the elastic moduli of cancer and healthy cells (approximately lying in the range 0.1–2 kPa and 0.5–7 kPa, respectively) experimentally obtained

Table 1
Synoptic table of the geometric and constitutive parameters of the model.

CSK tensegrity structure				
	Young modulus [GPa]	Poisson ratio [–]	Rest length [μm]	Reference area [nm^2]
Microtubules	1.2 (Gittes, 1993)	0.4	12	190 (Gittes, 1993)
Microfilaments	2.6 (Gittes, 1993)	0.4		18 (Gittes, 1993)

Cellular and extracellular environment				
	Young modulus [kPa]	Poisson ratio [–]	Density [kg/μm^3]	Damping coefficients
Nucleus	1.48 (Kim et al., 2011)	0.5 (Geltmeier et al., 2015)	1.30E−15 (Geltmeier et al., 2015)	
Cytosol	1.48	0.5 (Geltmeier et al., 2015)	1.05E−15 (Geltmeier et al., 2015)	α=6.6 β=0.02
Plasma membrane	1.48	0.45	1.05E−15	
ECM	15 (Nebuloni et al., 2016)	0.5	1.05E−15	
Tumor PCM	0.1 (Ahmadzadeh et al., 2017)	0.5	1.05E−15	

from a vast variety of literature works, as also synoptically $h = \sqrt{3}L_t\lambda_t^*/2$ reportedin Fraldi et al. (2015). In (5), $A_{up} = \sqrt{3}L_2(\lambda^{*t})^2/32$ and $\gamma = 3\sqrt{3}/t$ are geometrical parameters representing the upper triangle area (shown in Fig. 2B) and the height of the tensegrity in the unloaded prestretched configuration.

Implementing the tensegrity structure into the FE cell model. Specific stiffness values can be provided to tumor and healthy cells through the nonlinear model presented, to also meet the recent *in vitro* and *ex vivo* experiments evidencing that tumor cells result 70% more compliant than the healthy counterpart (Fraldi et al., 2017). From a mechanical standpoint, this higher deformability has been associated to the reorganization of the cytoskeleton (Fraldi et al., 2017, 2019; Palumbo et al., 2018) as well as to an increased migration potential in cells with tumorigenic phenotypes (Ketene et al., 2012). On the other hand, the stiffness gap between the cell types observed at the single scale level can play a key role to possibly discriminate cancer and healthy cells by inducing selective resonance-like phenomena also in a heterogeneous collective environment, in this way simulating – at least in principle – a focused targeting of *in situ* cancer cells and overcoming the acknowledged limitations of the studies on single-cells (Fraldi et al., 2017). Also, the regulation of the pre-stretch allows a rigidity tuning of the TS, in this way covering the most of cell lines measured mechanical properties and so having the possibility of considering several types of cells.

The finite element tensegrity struts and cables have been meshed with 3D bar elements, with three degrees of freedom at each node

( )

(LINK180) as $\mathbf{u} = u_x, u_y, u_z$. Tension-only response has been prescribed to the cables and geometric nonlinearity has been also considered (Plešek and Kruisová, 2006). With reference to the geometric and material parameters of Table 1, the pre-stretch values of $\lambda^*_f = 1.01$ $\lambda^*_f = 1.16$ have been assigned to cancer and healthy cells, respectively, determined in a way that the two cell types showed a difference in terms of global stiffness of about 70%, with minimal volume difference (Fig. 2A and B). By invoking the equilibrium equation (3), the adopted filament pre-stretches correspond to pre-contraction levels of $\lambda^*_t = 0.995$ and $\lambda^*_t = 0.928$ in the struts of the tumor and healthy cell tensegrities, respectively.

2.1.2. FE modeling of cell membrane, cytoplasm and internal nucleus

The volume underlined by each tensegrity has been meshed with 3D tetrahedral elements (SOLID185), while the delimiting external surface of the TS – individuated by the areas formed by its nodes – has been discretized with shell elements (SHELL181), including both membrane and bending capabilities. In order to guarantee that the response of tumor and healthy cells is mainly discriminated by their CSK, both cancerous and normal cells have been provided with analogous cytosol and membrane mechanical properties, given in terms of Young's modulus and Poisson's ratio. In particular, an incompressible value for the Poisson's ratio is considered, while the elastic modulus is of the order of units of kPa, the specific coefficients of Table 1 making reference to hepatic cell lineages (Kim et al., 2011). Furthermore, to also include the cell nucleus, a spherical region of elements with higher density has been placed at the center of each cell (see Fig. 1), with an

average diameter of about 10 μm for both the cell types and a density value approximately 30% greater than the other plasmatic phase, as also found in literature (Michelet-Habchi et al., 2005). Although the inclusion of viscoelasticity is expected not to drastically modify the frequency band of interest, when the damping of the cytosol is explicitly taken into account in the simulations, proper Rayleigh-type damping coefficients for the mass (α) and the stiffness (β) are assigned to the material parameters of the cytoplasm elements, their specific values being reported in Table 1.

2.1.3. The cell-ECM coupling at the interface

Cell agglomerates are constituted of multicellular populations that inhabit the extracellular solid environment. Accordingly, an ECM layer enveloping each cell was introduced, so that the single structural unit of the mass is composed by the cell-ECM system. Attention has been paid for both the mechanical characterization of the extracellular layers for tumor and healthy cells, as well as the form-finding of such units, in order to define a shape that permitted the full tessellation of the space.

Several recent literature works provide different values of ECM stiffness for healthy and tumor tissues (Schrader et al., 2011; Nebuloni et al., 2016; Tilghman et al., 2010), an increased environmental rigidity constituting itself a potential mechanical signaling for enhancing tumor cell proliferation and migration. In the model at hand, we consider multicellular aggregates in which tumor and healthy cells coexist in order to examine the differential response of cells to dynamic stimulation. Therefore, with the aim to analyze the cells-specific behavior under vibration, a common ECM stiffness was assumed. However, at the cell-ECM interface, dissimilar behaviors occur. Differently from the healthy cells, anchored at the matrix under homeostatic conditions, the more invasive tumor cells indeed show increased motility and alterations in metabolic activity, to sustain detachment from the ECM and initiate migration (Mason et al., 2017; Kim, 2001). This is enhanced by an over-expression of metalloproteinases-mediated degradation of peritumoral matrix (Martin, 1994; Ahmadzadeh et al., 2017) and a pronounced softening of the surrounding peri-cellular matrix (PCM), that mediates between the cell and the ECM and mechanically favors the movement of the more detached and poorly differentiated cancer cells through the ECM collagen networks, as reported in recent literature findings (Ahmadzadeh et al., 2017; Nijenhuis et al., 2012). All these considerations are taken into account in the present model by providing a greater mechanical compliance to the proximal extracellular elements that surround tumor cells. The mechanical properties used for the these extracellular elements are also reported in Table 1.

Furthermore, to build up the whole spheroidal structure by utilizing the most convenient topology of the periodic units, a 3D tessellation involving Kelvin's tetrakaidecahedron volumes has been adopted. This regular form, originally proposed by Lord Kelvin in 1887, results in fact the optimal natural space-filling shape possessing a minimal surface area (Thomson, 1887) and has been also recognized as natural configuration of some *in vivo* bulky structures, such as the stratified cells of mammalian epidermis (Yokouchi et al., 2016). Hence, the outer ECM layer has been conveniently modeled with this particular form, in this way fixing the geometry of the fundamental periodic unit of the aggregate. The overall assembling of a prescribed number of differently oriented KTK volumes with given cell-specific properties is directly related to the size of the tumor mass as well as to the tumor stage studied, in a way to obtain a multicellular and mechanically heterogeneous complex system.

2.2. Assembling of the aggregate at the multicellular level

The 3D tessellation has been developed thanks to a custom made algorithm in APDL Language, provided by the commercial software Ansys® (Ansys 15.0 User's Manual, 2013). The agglomerates are built up by setting different geometric and cell-specific mechanical parameters, linked to the size and the percentage of tumor cells therein contained. For the assembling phase, a random criterion for placing healthy and tumor cells has been defined through a custom made procedure that associates the type and the position of each unit to a three-dimensional matrix containing binary elements, viz 0 and 1, respectively representing healthy and cancer cells. Prescribed the *a priori* percentage of tumor cells, the 3D binary matrix was randomly filled and units located. The dimensions of such matrix is related to the size of the tumor spheroid. In particular, to contain the computational weight of the building procedure, the *in silico* aggregates have been constructed by adopting a 5 × 5 × 5 binary matrix, randomly distributing the different cell types in one of the octants of a Cartesian space with origin in the tumor center. The spheroidal shape has been therein obtained by making sure that all units lied into a spherical region of about 150 μm in diameter. This block was then replicated in the other octants, and an additional *ad hoc* algorithm was implemented to assign independent random rotations of 90 degrees with respect to each

Cartesian axis to any TS structure, in order to give random orientation to the cells and avoid possible effects in the response of the whole multicellular structure due to preferential directions. With reference to the cells dimensions reported in Table 1 and to the adopted spheroid diameters, this routine produced aggregates of 229 cells. Finally, to simulate the mechanical interaction of an *in vivo* tumor cell cluster with the external environment within which it is embedded, a coating of radially positioned link elements originates from the external nodes. Each element has been characterized with length, cross section and elastic properties to replicate in the best way the actual elastic features of the surrounding tissue.

2.3. Harmonic vibration analysis

The harmonic vibration analysis allows to evaluate the response of a structural system when subjected to sustained cyclic load, with the aim to predict the body dynamic behavior and appreciate possible resonance-like and fatigue phenomena. In the problem at hand, the numerical simulations have been conducted with the aid of the commercial FE-based code Ansys© (Ansys 15.0 User's Manual, 2013) and focused on the evaluation of the harmonic response of cell aggregates, in order to predict the effects of the ensemble when subjected to LITUS-induced mechanical vibrations. Although the way in which the mechanical vibrations due to ultrasound waves act on cells physiology still remains an open issue, several studies have explored the possibility to induce fatigue-like phenomena on cellular structures by means of US stimulation (Fraldi et al., 2015; Or and Kimmel, 2009). Particular attention is paid on the possibility to trigger resonance-like behavior at specific frequencies, in a way to disrupt the molecular complexes of tumor cells and cause cell structural death. In this sense, the aforementioned rigidity-based discrimination of tumor and healthy cells results diriment to explain their distinct sensitivity, and thus to understand how therapeutic ultrasounds interact with the different cell types in a way to envisage innovative strategies for selectively targeting malignant cells (Fraldi et al., 2015; Heyden and Ortiz, 2016). The recent literature provides several modeling approaches: specifically, efforts have been made to analytically characterize the in-frequency response of single cells and cell–cell systems by means of theoretical models that account for the intrinsic nonlinearity and viscoelasticity of cells components, also including cytoskeleton pre-stretch effects (Fraldi et al., 2015, 2017). Also, numerical models describing the harmonic response of single-cell structures have been encountered (Heyden and Ortiz, 2017; Geltmeier et al., 2015). With possible applications in mind, the present FE model studies the in-frequency response of cell aggregates, in which a high number of cells are grouped together to form a spheroidal structure. Cancer cells increase during tumor development and this was here simulated by varying the percentage of tumor cells within the spherical volume, this percentage becoming somehow an index of the tumor stage. In particular, in the reported analyses, the number of malignant cells increased from 25% of total cells up to 75%, as also shown in Fig. 3. The spheroid, obtained by a 3D tessellation of Kelvin's tetrakaidecahedron volumes, has been meshed with about 3×10^6 elements and about 5×10^5 nodes. The harmonic analyses have been carried out also by considering that the spherical mass is invested on a side by an US wave train, whose frequency lies into the range 19−150 kHz (Geltmeier et al., 2015; Johns, 2002). Within this band, different simulations have been performed in order to discriminate the cell responses, by tuning frequencies with steps of 9 kHz. The external nodes of the link elements, radially attached to the spheroid surface on the other extremity, are instead constrained by there imposing null nodal displacements.

3. Results and discussion

The harmonic behavior of spheroidal aggregates in response to possible US waves has been studied within a low frequency range of 19−150 kHz. In fact, preliminary calculations by hand, which consider spherical cells vibrating in a more rigid matrix, let to estimate thenatural frequency as $f \simeq d^{-1}\sqrt{E\rho^{-1}}$, $d$being the cell diameter. For the considered range of Young moduli E in Fig. 2 and with reference to 10 μm diameter cells with a water-like density, this rough formula returns an expected frequency interval of approximately 30−180 kHz. Starting from this, the numerical analyses aimed to investigate the possibility of realizing selective targeting or even ablative disruption of malignant cell population that inhabits a healthy tissue by using low intensity ultrasounds. For the assigned frequency spectrum, the dynamic stimulation of multicellular aggregates at different tumor percentages then focused on observing distinct sensitivity between the cancer and normal cells, thus scaling up the rigidity-dependent acoustic differences established at the single-cell scale for healthy and cancer cells towards the tissue level. This could enhance the understanding of the tumor masses–ultrasounds interactions, on which new therapeutic strategies are laying their groundwork with the goal of designing possible casespecific and less invasive treatments. To this purpose, the FE-spheroid external surface has been subjected to a sinusoidal (monochromatic) pressure, representing the US train, and cells vibration was considered by evaluating the displacements of the nuclei. The harmonic response of the cells has been studied by varying the fraction of tumor cells and tuning the pressure frequency with steps of 9 kHz. More in detail, we considered the mean displacements of the cells, denoted by $U_T$and $U_H$for tumor and healthy cells, respectively:

$$U_T = \frac{1}{N_T}\sum_{i=1}^{N_T}|\mathbf{u}_i| = \frac{1}{N_T}\sum_{i=1}^{N_T}\sqrt{(u_x^2)_i + (u_y^2)_i + (u_z^2)_i},$$
$$U_H = \frac{1}{N_H}\sum_{i=1}^{N_H}|\mathbf{u}_i| = \frac{1}{N_H}\sum_{i=1}^{N_H}\sqrt{(u_x^2)_i + (u_y^2)_i + (u_z^2)_i} \qquad (6)$$

in which $N_T$and $N_H$are the numbers of cancer and healthy cells. Results, shown in Fig. 3 with respect to spheroids constituted by the 25, 50 and 75% of cancer cells, are given in terms of:

- the mean displacement of the tumor and normal cells ensembles at the different frequencies considered, normalized with respect to the maximum displacement registered, say $\overline{U_T} = U_T/\max_{N_T\cup N_H}\{|\mathbf{u}_i|\}$ and $\overline{U_H} = U_H/\max_{N_T\cup N_H}\{|\mathbf{u}_i|\}$
- (the relative) differential displacement, evaluated as $U_R = U_T - U_H/U_H$, indicated above each histogram bar. Positive $U_R$suggest that tumor cells are more responsive to the considered frequency.

These two indicators let to evaluate the effects of US on the cells collective vibration, by discriminating tumor and healthy responses at a fixed frequency. In particular, the mean displacements bars can be correlated to the cell-specific deformation, which can induce the mechanical failure of the cell sub-structures when a critical threshold is overcome, while the relative displacements describe in which measure a given frequency produces greater vibration amplitudes in a selected cell population. This could be exploited to induce a resonant-type failure, which – combined with fatigue effects – could be at the basis of a selective attack of target cells. In terms of outcomes, by looking for instance at the aggregate containing the 25% of cancer cells in Fig. 3A, the mean displacement of tumor cells is maximum at 37 kHz; however, the measure of the relative displacements suggests a better efficiency in the band 60−90 kHz, in which U_R varies from +0.98 to +1.89, indicating that for such frequencies cancer cells sensitivity is higher than that one of the healthy cells. This suggests that, by properly setting the frequency of the US stimulation, the selective attack can be planned in order to avoid damage of the most of the normal cells. The right panel of Fig. 3A also shows the vector plots of nodal displacements

in correspondence of the frequencies provoking the maximum U_T and

U_H, respectively. Analogous considerations can been made for the 50% and the 75% tumor stages. In Fig. 3B, one can see that the mean displacement of malignant and healthy cells in the 50% tumor spheroid is highest at 19 kHz and exhibits positive values of relative vibrations up to about 80 kHz, with the maximum value of U_R occurring at 28 kHz. Similarly, in advanced stage (75% of cancer cells), Fig. 3C shows how cancer cells are more stimulated than normal cells practically into the same frequency interval, where the greatest values of both relative and mean tumor displacements are again reached at 28 and 19 kHz, respectively.

In the presented simulations, the frequency at which the relative motion U_R peaks instead in favor of the normal cells lays into the interval 127−135 kHz and keeps sufficiently separated from the cancer cells natural frequencies, that start from 80 kHz in the early stage (Fig. 3A) and settles at about 28 kHz for more invaded spheroids (Fig. 3B and C). The observed gaps ensure that the distinct sensitivity observed at the single cell scale for the malignant and normal cells occurs also at the aggregates level. Additional aspects can be taken into account in the present analyses in order to better describe tumor mechanical environment. The first one is the remodeling of the ECM during tumor development. The ECM stiffening in fact represents one of the most recognized determinants of tumor progression, which influences tumor pathophysiology and often constitutes a discriminant for cancer detection. Then, according to some literature measurements (Kim et al., 2011; Malandrino et al., 2018; Leight et al., 2017; Acerbi et al., 2015), ECM Young modulus was varied from 5 kPa, for the early-stage tumor aggregate, to 25 kPa for the tumor spheroid containing 75% of cancer cells. Also, cytosol viscoelasticity was explicitly considered by kindling proper damping coefficients into the numerical simulations. Results in Fig. 4 show that the frequency band at which tumor cells were more sensitive with respect to the healthy counterparts is essentially confirmed, the malignant cells resulting more responsive below 100 kHz, while the damping produces an attenuation of the displacement amplitudes and a spreading over the frequency range. In particular, Fig. 4 displays how the relative displacement of the tumor fraction peaks in the band 70−90 kHz in both fully elastic and viscoelastic aggregates with 25% of cancer cells, whilst the healthy ones exhibit highest relative vibrations at about 130−150 kHz. In the case of spheroids at 75% of cancer cells, the in-frequency discrimination between tumor
and healthy fractions accentuates since the peaks for cancer cells
move at 28−40 kHz for both the elastic and viscoelastic models, the resonance-like amplitude being attenuated in the latter one.

Importantly, all the frequencies determined here *in silico* – modeling the response of whole multicellular agglomerates – well meet some remarkable and very recent experiments performed on three-dimensional cultures of different tumor cell lines, in which an increased cancer cell death and delayed proliferation were induced through ultrasonic irradiation at low frequencies in the range 20−44 kHz (Geltmeier et al., 2015).

Several experimental findings are available in the literature with reference to tumor aggregates and masses subjected to sole US treatments, although the vast majority of research works analyze the co-action of ultrasounds with agent-loaded microbubbles (Wood and Sehgal, 2015). Nevertheless, some experimental studies interestingly match the outcomes of the above discussed numerical simulations. In the experimental study by Tijore et al. (2020), the acoustic exposure to low-frequency ultrasounds at 33 kHz and 120 kHz is indicated as a treatment condition that does not damage normal cells and increase the so called mechanoptosis in cancer cells. In particular, higher ultrasound-induced apoptotic levels were observed in both breast and ovarian cancer cell aggregates grown in matrigel as well as for tumors grown in chick embryo models. Noteworthy, enhanced apoptosis and damage events occurred also in human pancreatic tumor organoids having hundreds of microns in size. Also Bai et al. (2012) report that 21 kHz ultrasound sonication is able to induce a higher degree of cell
death in human prostate cancer cells, by observing increased damages
to cell membranes. Huang et al. (2013) registers a reduction of the growth rate of colon cancer in animal models irradiated with a 240 kHz transducer, then observing a recovery of the curve at about four weeks after the treatment. Furthermore, Barati et al. (2009) observed that a dual-frequency sonication at 150 kHz and 1 MHz induced an inhibitory effect on the growth of *in vivo* adenocarcinoma tumors. Sacks et al. (1983) were among the first to suggest the therapeutic potential of low intensity ultrasounds, by observing that sonication at 1 MHz caused damages in multicell tumor spheroids of about 150–200 μm in diameter. On the other hand, at frequencies above 1 MHz, the direct influence of ultrasound treatments on tumor aggregates seems to decrease. Previous works in fact testify a weaker sensitivity of cell aggregates to US treatments. In particular, Ter Haar et al. (1988) did not find significant changes in growth curves of 200−700 μm diameter spheroids after irradiation at 2.6 MHz and 37 °C, a delay being instead obtained when hyperthermia was combined with ultrasound exposure. No statistical significances in mammalian multicell tumor spheroids irradiated in the band 0.9−2.6 MHz were instead documented in Conger et al. (1981). Although further investigations and experiments are needed to clearly assess the frequency-dependent impact of the sole ultrasounds on tumor aggregates and spheroids, one may observes from the above discussed comparisons that a higher efficacy is documented when lower frequencies (of the order of tens/hundreds of kHz) are involved, their values being in good agreement with the findings of the presented theoretical predictions from numerical analyses.

It is also worth to notice that, differently from the literature models that focus on the single-cell behavior, the reported results are representative of the agglomerate response, by focusing on the overall motion of the cellular populations and including interactions between the cancer and healthy cells within the tissue as well as their interaction with the extra-cellular environment. The effort of introducing such a mechanically complex environment, in which each cell is reproduced in all its components and inserted in a heterogeneous medium, leads to understand which characteristics can be more prodromal to induce the selective damaging of *in situ* tumor cells through US at low frequencies, starting from the knowledge of tissue composition, mass size and elastic properties of the cell structures.

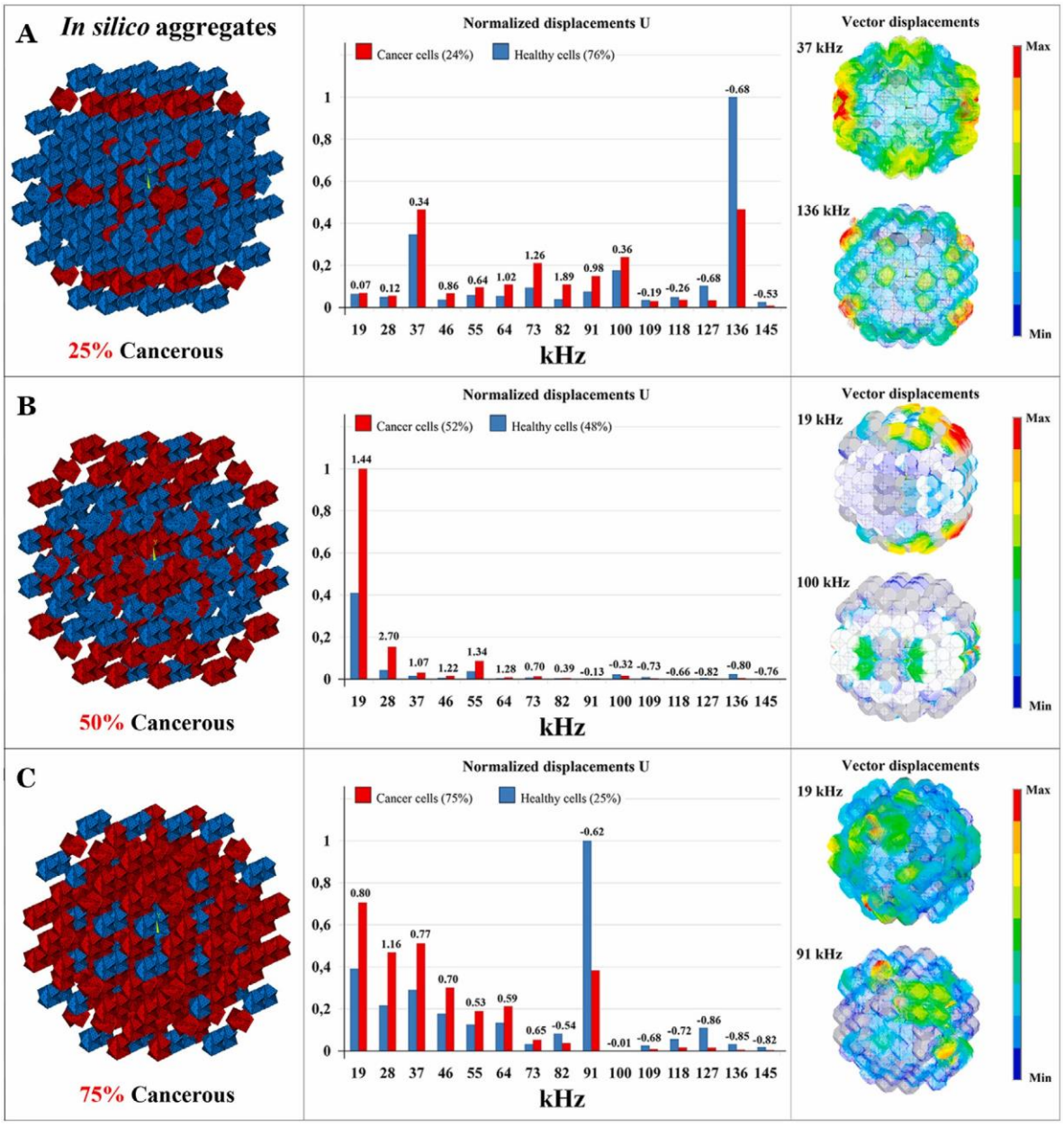

Fig. 3. (*Left column*) Representations of the aggregates with tumor (red) and healthy (blue) cells at different percentages. (*Middle column*) In-frequency evaluation of the mean and relative displacements of cancer and healthy cells in each tumor spheroid. (*Right column*) Vector plots of nodal displacements in correspondence of critical frequencies. A. 25%, B. 50% and C. 75% of cancer cells.

The US bioeffects on tumor and healthy cells can be associated to the theoretical outcomes at hand since the displacements of the cells centers can be related to the deformations experienced by the cells within the confined spheroids. High mean displacement values are indicative of the stretching of the cell substructures in response to the applied pressures, that could be critical to induce their disruption and therefore a mechanically-caused death of the cells. Elevated relative displacements imply a distinct average motion of the two cell types: this aspect could be instead exploited to predict stage-specific frequencies at which fatigue-like effects could be induced in the cell structures by means of prolonged sonication. Importantly, this mechanisms could concur in promoting favorable physiological phenomena in some cell lines, such as cells stress-induced quiescence, metabolic reduction and proliferation decrease as the direct effect of US-induced damages, as also discussed in the experimental literature (Wu, 2004; Wood and Sehgal, 2015; Tadayyon et al., 2015). Furthermore, the measures used to follow the cells vibrations can suggest different strategies for attacking tumor spheroids by opportunely setting the frequency and the planned time of treatment. In fact, by looking at the single-cell displacements in Fig. 5A, in the mass where cancer cells percentage is referred to the less aggressive tumor stage, different behaviors occur in correspondence of the target frequencies at which malignant cells are more responsive. In particular, Fig. 5A shows that, at 82 kHz, approximately the 42% of the tumor cells exhibits a displacement higher than the healthy cells' maximum displacement. No marked selection occurs at 37 kHz at which the highest U_T is determined, this implying that also a significant part of the healthy cells are inevitably hit. The characteristic frequencies obtained previously for the 50% and 75% tumor spheroids instead show greater percentages of selectively attacked tumor cells (see Fig. 5B and C), with the frequencies associated with maximum U_R keeping more efficient. Also, Fig. 5D shows the distribution of cells displacements (averaged over spherical crowns at different radii) as the effect of the propagation of the US wave through the interior of the cellular agglomerate.

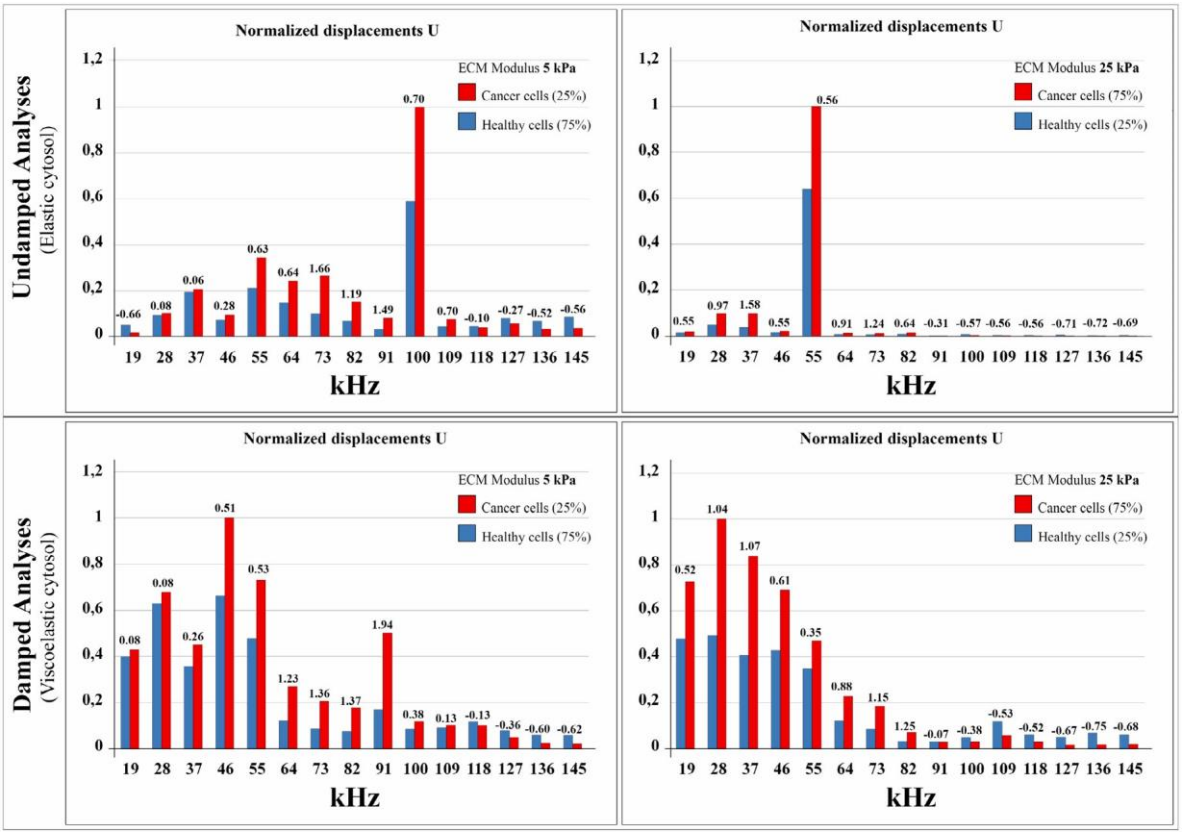

Fig. 4. Harmonic spectra of heterotypic spheroids with 25% and 75% of cancer cells, including the effects of ECM stiffening and damping due to viscoelasticity of the cytosol.

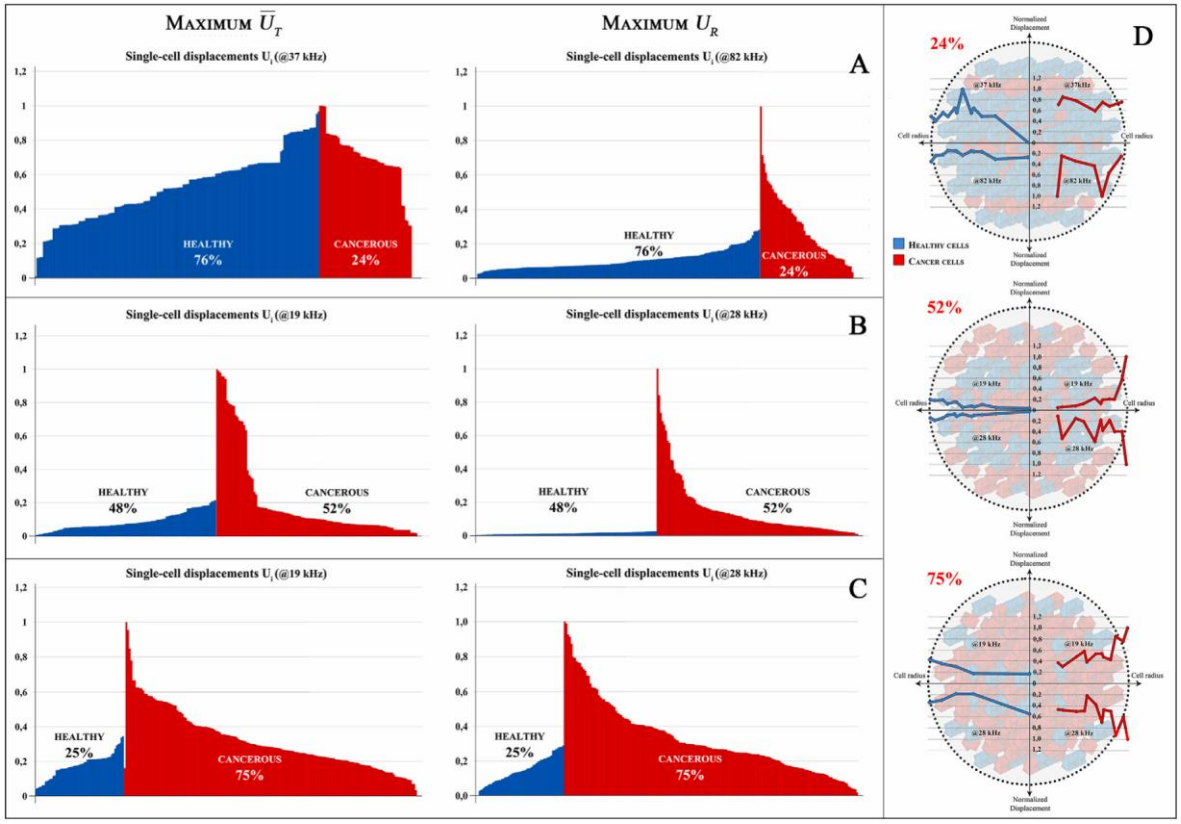

Fig. 5. Displacements of the single cells at prescribed frequencies. A. 25%, B. 50% and C. 75% of cancer cells. D. Radial distribution of displacements.

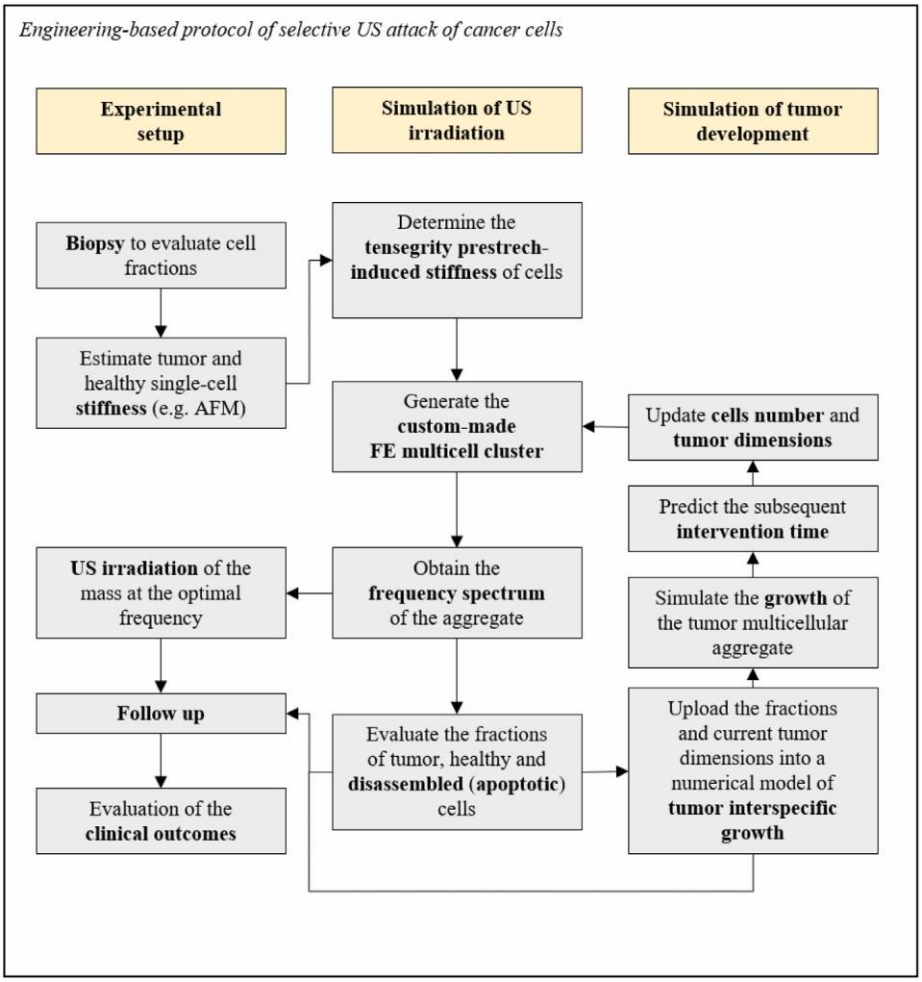

Fig. 6. Engineering-based protocol for selective attack of *in situ* cancer cells.

All these outcomes could be used to tune the US frequency at which cancer cells can be mechanically attacked at a specific growth stage with greater efficiency, also with respect to the possibility of dosing the intensity and the duration of the US stimulation, as well as the number of the treatments. In fact, as also illustrated in the scheme of Fig. 6, an engineering based protocol of selective attack of *in situ* cancer cells can be envisaged by planning the time sequence and the frequency of US treatments on the basis of *in silico* custom-made simulations. These ones need preliminary exams that allow to estimate the initial cell fractions and the cell pre-stretch-induced stiffness to be uploaded in the FE aggregate model and obtain its frequency spectrum and especially the optimal frequency for the current treatment. In addition, FE analyses return an estimation of the remaining tumor and healthy viable cells as well as of the disrupted apoptotic cells (that *de facto* represents a third species with different elastic properties because they present a disassembled cytoskeleton). The latter outcomes could be then exploited to simulate the subsequent tumor development, for example by means of *ad hoc* continuum models for describing interspecific tumor growth by means of an evolutionary framework (see e.g. Guiot et al., 2006; Carotenuto et al., 2018; Fraldi and Carotenuto, 2018; Carotenuto et al., 2021), in order to plan the time and the US parameters of the next treatment on the basis of the predicted tumor aggressiveness and by taking into account the growth-induced modifications of tumor tissue elasticity (Carotenuto et al., 2019). By therefore returning to the FE model a projection of the species fractions and the updated tumor dimensions, a new optimal LITUS frequency can be computed and administrated to the *in vivo* mass at the established time. In this way, numerical simulations – that provide the integration of different biomechanical models – can aid the optimization of a future possible therapeutic protocol able to suggest, at a prescribed tumor stage, which frequency ranges return the best possible trade-off between the death of cancer cells and the damage provoked to the healthy counterpart, and also which can be the most suitable time of sonication on the basis of cancer cells growth potential. With respect to the thermal damages to the tissue, thermal degeneration could have unfavorable clinical implications and induce the adverse mechanical remodeling of tissue elasticity, by altering its acoustic properties. However, for the standard powers used in the LITUS-based experiments (Geltmeier et al., 2015), these effects are limited at the frequencies of interest.

4. Conclusions

We presented an *in silico* fully parametric model aimed to replicate the harmonic response of realistic multicellular aggregates. Varying the ratio of tumor cells, target frequencies at which they can be selectively attacked by preserving the most of the surrounding healthy tissue have been identified. This effect is expected to cause mechanical lysis of cancer cells due to stresses induced by micro-vibration, as well as to alter some mechano-biological processes influenced by the stretching of the cytoskeleton and nucleus that are at the basis of cells activities and, in turn, of tumor development. Analyses were carried out by automatically managing the dimension and composition of the mass, in terms of cancer cells percentage. Spherical constructs were here considered to have the simplest model of multicellular aggregate, but the proposed strategy could be easily generalized to more complex tumor geometries. In this way, the effects of ultrasounds at single-cell scale were extended to configurations more close to *in vivo* situations. The results show that both selective targeting and attack of cancer

cells can be envisaged also when cell populations inhabit the same region and interact each other and with the extra-cellular matrix. In particular, the first outcomes suggest that mechanical resonance of cancer cells might still occur at frequencies compatible with those characterizing LITUS, also in case of coexistence of different cell phenotypes and constrained environmental conditions. On these bases, further numerical analyses could be planned to build up a biomechanically-driven strategy capable to suggest the optimal stage-dependent frequencies that maximize the outcomes of possible ultrasound treatments for experiments and future applications.

It is worth to highlight that, in the vast majority of the cases of interest, cells are interspersed with the synthesized matrix components. This implies that the overall mechanical properties and the dynamic response of tumor masses, from the initial stages in which they are formed by cell aggregates up to spheroids and tissues, are strongly influenced by the presence of the extracellular matrix during tumor development, in terms of both its own stiffness (which is in turn modified by the interaction with cancer cells) and cell-ECM connections. However, other interesting cases could be envisaged by grouping cells without considering ECM, a situation for instance encountered when cells form monolayers and are bulky organized such as in epidermis, or even in some *in vitro* constructs. To this regard, more direct cell– cell interactions could be also considered by including cell clusters forming within the multicell heterotypic spheroids, by taking into account irregular shapes and cell distributions as well as cell–cell junctions through proper elastic links, which are all factors inducing possible modifications of the vibration mechanisms. Although further efforts have to be made, it is however felt that the present modeling approach could contribute to make a further step towards the setting of engineered protocols to be translated in precise medicine.

CRediT authorship contribution statement

Massimiliano Fraldi: Conceptualization, Writing - review & editing, Supervision. **Arsenio Cutolo:** Investigation, Formal analysis, Software, Validation. **Angelo Rosario Carotenuto:** Formal analysis, Validation, Methodology, Writing. **Stefania Palumbo:** Investigation, Methodology, Validation. **Nicola Pugno:** Conceptualization, Review & editing.

Declaration of competing interest

The authors declare that they have no known competing financial interests or personal relationships that could have appeared to influence the work reported in this paper.

Acknowledgments

Compliance with Ethical Standards: This study was funded by the Italian Ministry of Education, Universities and Research through the grants: ''Integrated mechanobiology approaches for a precise medicine in cancer treatment, Italy'' (award number: PRIN-20177TTP3S) and ''Micromechanics and robotics for diagnosis and therapy in prostate cancer, Italy'' (award number: PON-ARS01_01384). A.R.C. also acknowledges support from PON-AIM1849854-1.

Appendix

Self-equilibrated tensegrity and kinematics of the TS contraction

Because of the geometrical symmetry, the coordinates of all nodes – in the Cartesian system identified by the unit vectors $\{\mathbf{e}_1,\mathbf{e}_2,\mathbf{e}_3\}$ – are defined by rigid transformations of a given node position vector, e.g.

$$)^{T}$$
$$_1 = L_t^*\left(\frac{1}{2}, \frac{1}{4}\right)\mathbf{p} \qquad _{-}, 0 \qquad , \mathbf{p}_2 = \mathbf{R}_x\mathbf{p}_1,\ \mathbf{p}_{5,6} = \mathbf{P}_\pi\mathbf{p}_{1,2},$$
$$\mathbf{p}_{9,10} = \mathbf{P}_\pi\mathbf{p}^{5,6} = \mathbf{P}_\pi^2\mathbf{p}_{1,2}, \qquad \text{(A.1)}$$
$$\mathbf{p}_{3,4} = \mathbf{R}_y\mathbf{p}_{1,2},\ \mathbf{p}_{7,8} = \mathbf{P}_\pi\mathbf{p}_{3,4} = \mathbf{P}_\pi\mathbf{R}_y\mathbf{p}_{1,2},\ \mathbf{p}_{11,12} = \mathbf{P}_\pi\mathbf{p}_{7,8} = \mathbf{P}_{2\pi}\mathbf{R}_y\mathbf{p}_{1,2}$$

where $L^*_t = \lambda^*_t L_t$ is the pre-stretched length of the tubules, $\mathbf{P}_\pi$ is a permutation matrix, while $\mathbf{R}_x$ and $\mathbf{R}_y$ are reflection matrices with

$$[\qquad]^{T}$$

respect to the axes x and y, respectively given by $\mathbf{P}_\pi = \mathbf{e}_3\mathbf{e}_1\mathbf{e}_2$, $\mathbf{R}_x = \mathbf{I} - 2\mathbf{e}_1 \otimes \mathbf{e}_1$ and $\mathbf{R}_y = \mathbf{I} - 2\mathbf{e}_2 \otimes \mathbf{e}_2$. In absence of external applied forces, equilibrium reads:

$$\sum_j N_{ij}^* \frac{\mathbf{p}_j - \mathbf{p}_i}{\|\mathbf{p}_j - \mathbf{p}_i\|} = \mathbf{0}, \qquad \forall i = 1,\dots,12 \qquad \text{(A.2)}$$

with the summation extended to all nodes j connected to the node i by an element ij and N_{ij}^* being the axial force that stresses that element. The symmetry of the module also returns homogeneous pre-stretches – and so pre-stresses – in both struts and cables. To instead simulate the imposed TS contraction, defined in terms of the nodes displacements $\mathbf{v}_k = \{u_k, v_k, w_k\}$, a vertical downward displacement is assigned to the upper nodes 1,5,9 of the tensegrity structure (see Fig. 2A), while the nodes 4,8,12 are anchored to the substrate. In such a way, the unknowns of the problem are the displacements' Cartesian components of the nodes belonging to the middle hexagon and the sole in-plane components of the upper nodes (refer to Fig. 2B). In order to minimize the number of the unknowns, a symmetry-preserving deformation has been imagined. In particular, the middle nodes (forming the middle hexagon shown in Fig. 2B) at the same height are assumed to share the same vertical displacement, i.e. the z_R-components of displacement of the nodes 3,7,11 and of the nodes 2,6,10 are:

$w_{HT} := w_3 = w_7 = w_{11}$ and $w_{HB} := w_2 = w_6 = w_{10}$, (A.3) where the subscripts HT and HB respectively refer to the upper and the lower nodes of the middle hexagon. Also, the symmetry implies that the radial and tangential displacements are equal still for the nodes 3,7,11 and 2,6,10 of the hexagon, respectively, this consideration being valid also for nodes 1,5,9. This is accounted by setting a local system

$$\{\quad\}$$

of polar coordinates lying in the x_R, y_R plane, centered at each of these nodes. Then, by indicating the shared radial and tangential displacements of the ith node with d_{ri} and d_{ti} in the local frames, the respective Cartesian nodal displacements u_i and v_i along the axes x_R and y_R result:

$$\begin{bmatrix} \\ u_i \\ \\ \end{bmatrix} = \mathbf{R}(\alpha_i)\begin{bmatrix} \\ d_{ti} \\ \\ \end{bmatrix}, \text{ with } \mathbf{R}(\alpha_i) := \begin{bmatrix} \\ \cos\alpha_i & \sin\alpha_i \\ v_i & d_{ri} & -\sin\alpha_i & \cos\alpha_i \end{bmatrix}, \quad \text{(A.4)}$$

where $d_{ri} := d_{rUT}$ and $d_{ti} := d_{tUT}$ for $i = \{1,5,9\}$, $d_{ri} := d_{rHT}$ and $d_{ti} := d_{tHT}$ for $i = \{3,7,11\}$, $d_{ri} := d_{rHB}$ and $d_{ti} := d_{tHB}$ for $i = \{2,6,10\}$, while $\mathbf{R}(\alpha_i)$ is the clockwise rotation matrix defined in

(A.4)$_2$ as a function of the angle α_i, defined with respect to the axis y_R and depending on the position of the specific node in the Cartesian frame:

$$\alpha_{\{1,5,9\}} = 2\pi - \arccos\left(\frac{\{5,-2,-1\}}{\sqrt{\quad}}\right), \qquad \alpha_{\{2,3,6,7,10,11\}} = \{7,1,3,9,11,5\}\frac{\pi}{6} \qquad \text{(A.5)}$$

Under these considerations, the unknowns of min problem $\mathbf{v}_i = \min_{\mathbf{v}_i} \Psi$ reduce to eight, namely d_{rUT}, d_{tUT}, d_{rHT}, d_{tHT}, d_{rHB}, d_{tHB}, w_{HT}, w_{HB}, while the vertical displacement w_{up} of the upper equilateral triangle is prescribed and the displacements components of the lower nodes fixed to 0.

References

Acerbi, I., Cassereau, L., Dean, I., Shi, Q., Au, A., Park, C., Chen, Y., Liphardt, J., Hwang, E., Weaver, V., 2015. Human breast cancer invasion and aggression correlates with ecm stiffening and immune cell infiltration. Integr. Biol. 7 (10), 1120–1134.

Ahmadzadeh, H., Webster, M.R., Behera, R., Valencia, A.M.J., Wirtz, D., Weeraratna, A.T., Shenoy, V.B., 2017. Modeling the two-way feedback between contractility and matrix realignment reveals a nonlinear mode of cancer cell invasion. Proc. Natl. Acad. Sci. 114 (9), E1617–E1626. http://dx.doi.org/10.1073/ pnas.1617037114.

Ansys 15.0 User's Manual, 2013. ANSYS Mechanical User's Guide, Release 15.0 Edition. ANSYS, Inc.

Bai, W.-K., Wu, Z.-H., Shen, E., Zhang, J.-Z., Hu, B., 2012. The improvement of liposome-mediated transfection of pEGFP DNA into human prostate cancer cells by combining low-frequency and low-energy ultrasound with microbubbles. Oncol. Rep. 27 (2), 475–480.

Baker, K., Robertson, V., Duck, F., 2001. A review of therapeutic ultrasound: Biophysical effects. Phys. Therapy http://dx.doi.org/10.1093/ptj/81.7.1351.

Barati, A.H., Mokhtari-Dizaji, M., Mozdarani, H., Bathaie, S.Z., Hassan, Z.M., 2009. Treatment of murine tumors using dual-frequency ultrasound in an experimental in vivo model. Ultrasound Med. Biol. 35 (5), 756–763.

Carotenuto, A., Cutolo, A., Palumbo, S., Fraldi, M., 2019. Growth and remodeling in highly stressed solid tumors. Meccanica 54 (13), 1941–1957.

Carotenuto, A.R., Cutolo, A., Palumbo, S., Fraldi, M., 2021. Lyapunov stability of competitive cells dynamics in tumor mechanobiology. Acta Mech. Sinica 1–20.

Carotenuto, A., Cutolo, A., Petrillo, A., Fusco, R., Arra, C., Sansone, M., Larobina, D., Cardoso, L., Fraldi, M., 2018. Growth and in vivo stresses traced through tumor mechanics enriched with predator-prey cells dynamics. J. Mech. Behav. Biomed. Mater. http://dx.doi.org/10.1016/j.jmbbm.2018.06.011.

Carotenuto, A.R., Lunghi, L., Piccolo, V., Babaei, M., Dayal, K., Pugno, N., Zingales, M., Deseri, L., Fraldi, M., 2020. Mechanobiology predicts raft formations triggered by ligand-receptor activity across the cell membrane. J. Mech. Phys. Solids 141, 103974.

Chen, S., 2017. GPCRs and cancer. Front. Genetics 8, 162.

Chumakova, O.V., Liopo, A.V., Evers, B.M., Esenaliev, R.O., 2006. Effect of 5fluorouracil, optison and ultrasound on MCF-7 cell viability. Ultrasound Med. Biol. 32 (5), 751–758. http://dx.doi.org/10.1016/j.ultrasmedbio.2006.01.011.

Conger, A.D., Ziskin, M.C., Wittels, H., 1981. Ultrasonic effects on mammalian multicellular tumor spheroids. J. Clin. Ultrasound 9 (4), 167–174.

Cross, S.E., Jin, Y.-S., Rao, J., Gimzewski, J.K., 2007. Nanomechanical analysis of cells from cancer patients. Nature Nanotechnol. 2 (12), 780–783. http://dx.doi.org/10. 1038/nnano.2007.388.

Faria, E.C., Ma, N., Gazi, E., Gardner, P., Brown, M., Clarke, N.W., Snook, R.D., 2008. Measurement of elastic properties of prostate cancer cells using AFM. Analyst 133, 1498–1500. http://dx.doi.org/10.1039/B803355B.

Feng, Y., Tian, Z.-M., Wan, M.-X., Zheng, Z.-B., 2008. Low intensity ultrasound-induced apoptosis in human gastric carcinoma cells. World J. Gastroenterol. 14 (31), 4873. http://dx.doi.org/10.3748/wjg.14.4873.

Fraldi, M., Carotenuto, A.R., 2018. Cells competition in tumor growth poroelasticity. J. Mech. Phys. Solids 112, 345–367. http://dx.doi.org/10.1016/j.jmps.2017.12.015.

Fraldi, M., Cugno, A., Carotenuto, A.R., Cutolo, A., Pugno, N.M., Deseri, L., 2017. Smallon-large fractional derivative–based single-cell model incorporating cytoskeleton prestretch. J. Eng. Mech. 143 (5), D4016009. http://dx.doi.org/10.1061/(asce)em. 1943-7889.0001178.

Fraldi, M., Cugno, A., Deseri, L., Dayal, K., Pugno, N.M., 2015. A frequency-based hypothesis for mechanically targeting and selectively attacking cancer cells. J. R. Soc. Interface 12 (111), 20150656. http://dx.doi.org/10.1098/rsif.2015.0656.

Fraldi, M., Palumbo, S., Carotenuto, A., Cutolo, A., Deseri, L., Pugno, N., 2019. Buckling soft tensegrities: Fickle elasticity and configurational switching in living cells. J. Mech. Phys. Solids 124, 299–324. http://dx.doi.org/10.1016/j.jmps.2018.10.017.

Geltmeier, A., Rinner, B., Bade, D., Meditz, K., Witt, R., Bicker, U., BludszuweitPhilipp, C., Maier, P., 2015. Characterization of dynamic behaviour of MCF7 and MCF10a cells in ultrasonic field using modal and harmonic analyses. In: Chang, Y.J. (Ed.), PLOS ONE 10 (8), e0134999. http://dx.doi.org/10.1371/journal.pone. 0134999.

Gittes, F., 1993. Flexural rigidity of microtubules and actin filaments measured from thermal fluctuations in shape. J. Cell Biol. 120 (4), 923–934. http://dx.doi.org/10. 1083/jcb.120.4.923.

Guiot, C., Pugno, N., Delsanto, P.P., 2006. Elastomechanical model of tumor invasion. Appl. Phys. Lett. 89 (23), 233901.

Haag, P., Frauscher, F., Gradl, J., Seitz, A., Schäfer, G., Lindner, J.R., Klibanov, A.L., Bartsch, G., Klocker, H., Eder, I.E., 2006. Microbubble-enhanced ultrasound to deliver an antisense oligodeoxynucleotide targeting the human androgen receptor into prostate tumours. J. Steroid Biochem. Molecular Biol. 102 (1), 103–113. http: //dx.doi.org/10.1016/j.jsbmb.2006.09.027, Proceedings of the 17th International Symposium of The Journal of Steroid Biochemistry and Molecular Biology. RECENT ADVANCES IN STEROID BIOCHEMISTRY AND MOLECULAR BIOLOGY (Seefeld, Tyrol, Austria 31 May-3 June 2006).

Heyden, S., Ortiz, M., 2016. Oncotripsy: Targeting cancer cells selectively via resonant harmonic excitation. J. Mech. Phys. Solids 92, 164–175. http://dx.doi.org/10.1016/ j.jmps.2016.04.016.

Heyden, S., Ortiz, M., 2017. Investigation of the influence of viscoelasticity on oncotripsy. Comput. Methods Appl. Mech. Engrg. 314, 314–322. http://dx.doi.org/ 10.1016/j.cma.2016.08.026.

Huang, P., You, X., Pan, M., Li, S., Zhang, Y., Zhao, Y., Wang, M., Hong, Y., Pu, Z., Chen, L., et al., 2013. A novel therapeutic strategy using ultrasound mediated microbubbles destruction to treat colon cancer in a mouse model. Cancer Lett. 335 (1), 183–190.

Ingber, D.E., 1993. Cellular tensegrity: defining new rules of biological design that govern the cytoskeleton. J. Cell Sci..

Ingber, D.E., Wang, N., Stamenović, D., 2014. Tensegrity, cellular biophysics, and the mechanics of living systems. Rep. Progr. Phys. 77 (4), 046603. http://dx.doi.org/ 10.1088/0034-4885/77/4/046603.

Innamorati, G., Valenti, M.T., Giovinazzo, F., Dalle Carbonare, L., Parenti, M., Bassi, C., 2011. Molecular approaches to target GPCRs in cancer therapy. Pharmaceuticals 4 (4), 567–589.

Johns, L.D., 2002. Nonthermal effects of therapeutic ultrasound: the frequency resonance hypothesis. J. Athl. Train 37 (3), 293–299.

Ketene, A.N., Schmelz, E.M., Roberts, P.C., Agah, M., 2012. The effects of cancer progression on the viscoelasticity of ovarian cell cytoskeleton structures. Nanomed. Nanotechnol. Biol. Med. 8 (1), 93–102. http://dx.doi.org/10.1016/j.nano.2011.05. 012.

Kim, D., 2001. Akt/PKB promotes cancer cell invasion via increased motility and metalloproteinase production. The FASEB J. 15 (11), 1953–1962. http://dx.doi. org/10.1096/fj.01-0198com.

Kim, Y., Kim, M., Shin, J.H., Kim, J., 2011. Characterization of cellular elastic modulus using structure based double layer model. Med. Biol. Eng. Comput. 49 (4), 453–462. http://dx.doi.org/10.1007/s11517-010-0730-y.

Korayem, M., Heidary, K., Rastegar, Z., 2020. The head and neck cancer (HN-5) cell line properties extraction by AFM. J. Biol. Eng. 14 (1), 1–15.

Korayem, M.H., Rastegar, Z., 2019. Experimental characterization of MCF-10a normal cells using AFM: Comparison with MCF-7 cancer cells. Mol. Cell. Biomech. 16 (2), 109.

Korayem, M., Shahali, S., Rastegar, Z., 2018a. Experimental determination of folding factor of benign breast cancer cell (MCF10a) and its effect on contact models and 3D manipulation of biological particles. Biomech. Model. Mechanobiol. 17 (3), 745–761.

Korayem, M.H., Sooha, Y., Rastegar, Z., 2018b. MCF-7 cancer cell apparent properties and viscoelastic characteristics measurement using AFM. J. Brazilian Soc. Mech. Sci. Eng. 40 (6), 1–11.

Leight, J.L., Drain, A.P., Weaver, V.M., 2017. Extracellular matrix remodeling and stiffening modulate tumor phenotype and treatment response.

Lejbkowicz, F., Salzberg, S., 1997. Distinct sensitivity of normal and malignant cells to ultrasound in vitro. Environ. Health Perspect. 105 (Suppl 6), 1575–1578. http: //dx.doi.org/10.1289/ehp.97105s61575.

Lejbkowicz, F., Zwiran, M., Salzberg, S., 1993. The response of normal and malignant cells to ultrasound in vitro. Ultrasound Med. Biol. 19 (1), 75–82. http://dx.doi.org/ 10.1016/0301-5629(93)90020-o.

Lekka, M., Laidler, P., Gil, D., Lekki, J., Stachura, Z., Hrynkiewicz, A.Z., 1999. Elasticity of normal and cancerous human bladder cells studied by scanning force microscopy. Eur. Biophys. J. 28 (4), 312–316. http://dx.doi.org/10.1007/s002490050213.

Lekka, M., Pogoda, K., Gostek, J., Klymenko, O., Prauzner-Bechcicki, S., WiltowskaZuber, J., Jaczewska, J., Lekki, J., Stachura, Z., 2012. Cancer cell recognition – mechanical phenotype. Micron 43 (12), 1259–1266. http://dx.doi.org/10.1016/j. micron.2012.01.019, Special issue on AFM in Biology & Bionanomedicine.

Li, F., Jin, L., Wang, H., Wei, F., Bai, M., Shi, Q., Du, L., 2014. The dual effect of ultrasound-targeted microbubble destruction in mediating recombinant adenoassociated virus delivery in renal cell carcinoma: transfection enhancement and tumor inhibition. J. Gene Med. 16 (1–2), 28–39. http://dx.doi.org/10.1002/jgm. 2755.

Malandrino, A., Mak, M., Kamm, R.D., Moeendarbary, E., 2018. Complex mechanics of the heterogeneous extracellular matrix in cancer. Extreme Mech. Lett. 21, 25–34.

Martin, 1994. Nitric oxide decreases motility and increases adhesion in human breast cancer cells. Oncol. Rep..

Mason, J.A., Hagel, K.R., Hawk, M.A., Schafer, Z.T., 2017. Metabolism during ECM detachment: Achilles heel of cancer cells? Trends Cancer 3 (7), 475–481. http: //dx.doi.org/10.1016/j.trecan.2017.04.009.

Michelet-Habchi, C., Incerti, S., Aguer, P., Barberet, P., Gontier, E., Guinefolleau, T., Moretto, P., Pouthier, A., Pouthier, T., Smith, R., 2005. 3D imaging of microscopic structures using a proton beam. IEEE Trans. Nuclear Sci. 52 (3), 612–617. http: //dx.doi.org/10.1109/tns.2005.851411.

Mittelstein, D.R., Ye, J., Schibber, E.F., Roychoudhury, A., Martinez, L.T., Fekrazad, M.H., Ortiz, M., Lee, P.P., Shapiro, M.G., Gharib, M., 2020. Selective ablation of cancer cells with low intensity pulsed ultrasound. Appl. Phys. Lett. 116 (1), 013701.

Mizrahi, N., Zhou, E.H., Lenormand, G., Krishnan, R., Weihs, D., Butler, J.P., Weitz, D.A., Fredberg, J.J., Kimmel, E., 2012. Low intensity ultrasound perturbs cytoskeleton dynamics. Soft Matter 8 (8), 2438. http://dx.doi.org/10.1039/ c2sm07246g.

Nebuloni, M., Albarello, L., Andolfo, A., Magagnotti, C., Genovese, L., Locatelli, I., Tonon, G., Longhi, E., Zerbi, P., Allevi, R., Podestà, A., Puricelli, L., Milani, P., Soldarini, A., Salonia, A., Alfano, M., 2016. Insight on colorectal carcinoma infiltration by studying perilesional extracellular matrix. Sci. Rep. 6 (1), http: //dx.doi.org/10.1038/srep22522.

Nijenhuis, N., Mizuno, D., Spaan, J.A.E., Schmidt, C.F., 2012. High-resolution microrheology in the pericellular matrix of prostate cancer cells. J. R. Soc. Interface 9 (73), 1733–1744. http://dx.doi.org/10.1098/rsif.2011.0825.

Ong, M.S., Deng, S., Halim, C.E., Cai, W., Tan, T.Z., Huang, R.Y.-J., Sethi, G., Hooi, S.C., Kumar, A.P., Yap, C.T., 2020. Cytoskeletal proteins in cancer and intracellular stress: A therapeutic perspective. Cancers 12 (1), 238.

Or, M., Kimmel, E., 2009. Modeling linear vibration of cell nucleus in low intensity ultrasound field. Ultrasound Med. Biol. 35 (6), 1015–1025. http://dx.doi.org/10. 1016/j.ultrasmedbio.2008.11.011.

Palumbo, S., Carotenuto, A.R., Cutolo, A., Deseri, L., Fraldi, M., 2018. Nonlinear elasticity and buckling in the simplest soft-strut tensegrity paradigm. Int. J. Non-Linear Mech. 106, 80–88. http://dx.doi.org/10.1016/j.ijnonlinmec.2018.08.011.

Pezo, R.C., Singer, R.H., 2008. Nuclear microenvironment in cancer diagnosis and treatment. J. Cell. Biochem. 104 (6), 1953–1963.

Plešek, J., Kruisová, A., 2006. Formulation, validation and numerical procedures for Hencky's elasticity model. Comput. Struct. 84 (17–18), 1141–1150. http://dx.doi. org/10.1016/j.compstruc.2006.01.005.

Prabhune, M., Belge, G., Dotzauer, A., Bullerdiek, J., Radmacher, M., 2012. Comparison of mechanical properties of normal and malignant thyroid cells. Micron 43 (12), 1267–1272. http://dx.doi.org/10.1016/j.micron.2012.03.023, Special issue on AFM in Biology & Bionanomedicine.

Sacks, P.G., Miller, M.W., Sutherland, R.M., 1983. Response of multicell spheroids to 1-MHz ultrasonic irradiation: cavitation-related damage. Radiat. Res. 93 (3), 545–559.

Sawai, Y., Murata, H., Koto, K., Matsui, T., Horie, N., Ashihara, E., Maekawa, T., Fushiki, S., Kubo, T., 2012. Effects of low-intensity pulsed ultrasound on osteosarcoma and cancer cells. Oncol. Rep. 28 (2), 481–486. http://dx.doi.org/10.3892/or. 2012.1816.

Schibber, E., Mittelstein, D., Gharib, M., Shapiro, M., Lee, P., Ortiz, M., 2020. A dynamical model of oncotripsy by mechanical cell fatigue: selective cancer cell ablation by low-intensity pulsed ultrasound. Proc. R. Soc. Lond. Ser. A Math. Phys. Eng. Sci. 476 (2236), 20190692.

Schrader, J., Gordon-Walker, T.T., Aucott, R.L., van Deemter, M., Quaas, A., Walsh, S., Benten, D., Forbes, S.J., Wells, R.G., Iredale, J.P., 2011. Matrix stiffness modulates proliferation, chemotherapeutic response, and dormancy in hepatocellular carcinoma cells. Hepatology 53 (4), 1192–1205. http://dx.doi.org/10.1002/hep. 24108.

Schuster, A., Schwab, T., Bischof, M., Klotz, M., Lemor, R., Degel, C., Schäfer, K.-H., 2013. Cell specific ultrasound effects are dose and frequency dependent. Annals Anatomy - Anat. Anz. 195 (1), 57–67. http://dx.doi.org/10.1016/j.aanat.2012.03. 008.

Tabuchi, Y., Takasaki, I., Zhao, Q.-L., Wada, S., Hori, T., Feril, L.B., Tachibana, K., Nomura, T., Kondo, T., 2008. Genetic networks responsive to low-intensity pulsed ultrasound in human lymphoma U937 cells. Cancer Lett. 270 (2), 286–294. http: //dx.doi.org/10.1016/j.canlet.2008.05.018.

Tadayyon, H., Sannachi, L., Sadeghi-Naini, A., Al-Mahrouki, A., Tran, W.T., Kolios, M.C., Czarnota, G.J., 2015. Quantification of ultrasonic scattering properties of in vivo tumor cell death in mouse models of breast cancer. Transl. Oncol. 8 (6), 463–473. http://dx.doi.org/10.1016/j.tranon.2015.11.001.

Ter Haar, G., Walling, J., Loverock, P., Townsend, S., 1988. The effect of combined heat and ultrasound on multicellular tumour spheroids. Int. J. Radiat. Biol. 53 (5), 813–827.

Thomson, W., 1887. LXIII.on the division of space with minimum partitional area. Phil. Mag. Ser. 5 24 (151), 503–514. http://dx.doi.org/10.1080/14786448708628135.

Tian, Z.-M., Wan, M.-X., Lu, M.-Z., Wang, X.-D., Wang, L., 2005. The alteration of protein profile of walker 256 carinosarcoma cells during the apoptotic process induced by ultrasound. Ultrasound Med. Biol. 31 (1), 121–128. http://dx.doi.org/ 10.1016/j.ultrasmedbio.2004.09.008.

Tijore, A., Margadant, F., Yao, M., Hariharan, A., Chew, C.A.Z., Powell, S., Bonney, G.K., Sheetz, M., 2020. Ultrasound-mediated mechanical forces selectively kill tumor cells. bioRxiv.

Tilghman, R.W., Cowan, C.R., Mih, J.D., Koryakina, Y., Gioeli, D., Slack-Davis, J.K., Blackman, B.R., Tschumperlin, D.J., Parsons, J.T., 2010. Matrix rigidity regulates cancer cell growth and cellular phenotype. In: Hotchin, N.A. (Ed.), PLoS ONE 5 (9), e12905. http://dx.doi.org/10.1371/journal.pone.0012905.

Tomizawa, M., Ebara, M., Saisho, H., Sakiyama, S., Tagawa, M., 2001. Irradiation with ultrasound of low output intensity increased chemosensitivity of subcutaneous solid tumors to an anti-cancer agent. Cancer Lett. 173 (1), 31–35. http://dx.doi.org/10.1016/S0304-3835(01)00687-5.

Wolfram Research, Inc., 2015. Mathematica. Wolfram Research, Inc..

Wood, A.K., Ansaloni, S., Ziemer, L.S., Lee, W.M.-F., Feldman, M.D., Sehgal, C.M., 2005. The antivascular action of physiotherapy ultrasound on murine tumors. Ultrasound Med. Biol. 31 (10), 1403–1410. http://dx.doi.org/10.1016/j.ultrasmedbio.2005.06. 008.

Wood, A.K., Sehgal, C.M., 2015. A review of low-intensity ultrasound for cancer therapy. Ultrasound Med. Biol. 41 (4), 905–928. http://dx.doi.org/10.1016/j. ultrasmedbio.2014.11.019.

Wu, F., 2004. Extracorporeal high intensity focused ultrasound ablation in the treatment of 1038 patients with solid carcinomas in China: an overview. Ultrasonics Sonochem. 11 (3–4), 149–154. http://dx.doi.org/10.1016/j.ultsonch.2004.01.011.

Yokouchi, M., Toru, A., van, L.M., J, T.R., Mayumi, K., Makoto, S., Mikio, F., Masayuki, A., Akiharu, K., Valerie, H., 2016. Epidermal cell turnover across tight junctions based on kelvin's tetrakaidecahedron cell shape. eLife 5 (eLife), http://dx.doi.org/10.7554/eLife.19593.